



Article

Solvent Effects on the Spin Crossover Properties of Iron(II) Imidazolyimine Complexes

Darunee Sertphon¹, Phimphaka Harding¹, Keith S. Murray² , Boujemaa Moubaraki², Suzanne M. Neville³, Lujia Liu⁴, Shane G. Telfer⁴ and David J. Harding^{1,*} 

- ¹ Functional Materials and Nanotechnology Center of Excellence, Walailak University, Thasala, Nakhon Si Thammarat 80160, Thailand; sdarunee3@gmail.com (D.S.); kphimpha@mail.wu.ac.th (P.H.)
² School of Chemistry, Monash University, Clayton, VIC 3800, Australia; keith.murray@monash.edu (K.S.M.); boujemaa.moubaraki@monash.edu (B.M.)
³ School of Chemistry, University of New South Wales, Sydney, NSW 2052, Australia; s.neville@unsw.edu.au
⁴ MacDiarmid Institute for Advanced Materials and Nanotechnology, Institute of Fundamental Sciences, Massey University, Palmerston North 4442, New Zealand; lujia.liu@northwestern.edu (L.L.); S.Telfer@massey.ac.nz (S.G.T.)
* Correspondence: h david@mail.wu.ac.th; Tel.: +66-75-672094

Received: 23 January 2019; Accepted: 20 February 2019; Published: 22 February 2019



Abstract: A series of Fe(II) complexes, *fac*-[Fe(4-ima-Bp)₃](Y)₂·sol (Y = ClO₄; sol = 3EtOH **1**, 3MeOH **2**; Y = BF₄; sol = EtOH·4H₂O **3**, 4H₂O **4** and 3.5MeCN **5**) have been prepared and structurally and magnetically characterized. The low temperature structures of **1**, **2** and **5** have been determined by X-ray crystallography with LS Fe(II) centres found in all cases. Extensive C–H···π interactions between the cations form 2D layers, which are linked to one another through N–H···O and O–H···O hydrogen bonds, resulting in high cooperativity. Despite **5** containing MeCN, N–H···O/F hydrogen bonds, and C–H···π and π–π interactions combine to give similar 2D layers. Magnetic measurements reveal moderately abrupt spin crossover for **1–4**; becoming more gradual and only 50% complete in **1** due to solvent loss. The MeCN solvate shows more gradual SCO and reinforces how subtle changes in packing can significantly influence SCO behaviour.

Keywords: spin crossover; iron(II) complexes; C–H···π interactions; magnetic properties; thermochromism

1. Introduction

Spin crossover (SCO) describes the interconversion between a high spin (HS) and low spin (LS) state induced by a range of external perturbations often temperature or light irradiation [1,2]. SCO in Fe(II) complexes with an octahedral geometry is dominant as it transforms a diamagnetic LS state (S = 0) to a paramagnetic HS state (S = 2) with a clear change in colour and lengthening of the Fe(II)-ligands bond distances [3–7]. Materials displaying SCO behaviour continue to be intensively studied due to their potential use as active components in memory, display and sensing devices [8–10] particularly photo-induced SCO complexes, or light-induced spin state trapping (LIESST) [11,12] which has been reported in many Fe(II) SCO systems.

Of the many iron(II) systems investigated those incorporating imidazole Schiff-base ligands have amongst the most varied SCO behaviours as exemplified in recent reviews by Kruger and Matsumoto [13,14]. In terms of mononuclear systems there are two basic designs one of which uses hexadentate ligands [15,16] and the other exploiting chelating imine ligands derived from an imidazolecarboxaldehyde. The ligand structures and abbreviations used in this article are shown in Chart 1. Amongst the first reports concerned [Fe{H₃(2-Me-im)₃-tren}]Cl·X (X = PF₆, AsF₆, SbF₆ and OTf) where the anion causes a change in magnetic behaviour from 50% SCO to abrupt and complete

SCO [17]. A feature of all the compounds are N-H...Cl hydrogen bonds that link the Fe(II) centres—this acts to enhance the communication pathways between SCO sites in the solid-state. Some years later, Seredyuk and co-workers studied $[\text{Fe}\{\text{N-}n\text{Bu-2-im}\}_3\text{-tren}]\text{(PF}_6)_2$, which exhibits SCO behaviour with thermal hysteresis sensitive to scan rate (i.e., 14 K at 4 K min⁻¹ and 41 K at 0.1 K min⁻¹) [18,19]. This measurement scan rate dependency is due to the kinetically-driven formation of two distinct LS phases which differ in butyl group conformation.

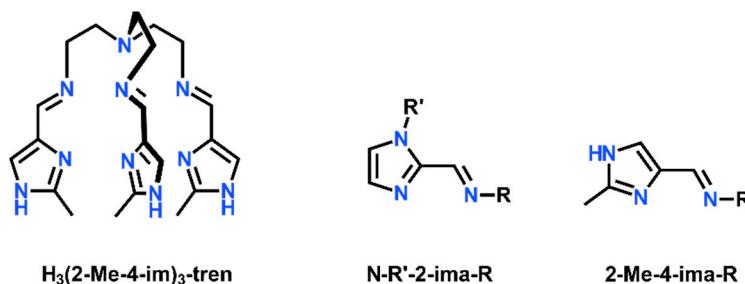


Chart 1. Structure of the common ligands used in mononuclear imidazole SCO systems.

SCO systems with chelating imidazole ligands are also well described with $[\text{Fe}(2\text{-Me-4-ima-CH}_2\text{CH}_2\text{py})_3](\text{X})_2$ ($\text{X} = \text{PF}_6, \text{ClO}_4, \text{BF}_4$) all showing abrupt SCO due to N-H...N hydrogen bonds involving the imidazole and pyridine [20]. Surprisingly, despite their different shapes and sizes the anion has little effect on the spin transition temperature. In 2011, Matsumoto et al. examined *fac*- $[\text{Fe}(2\text{-Me-4-ima-R})_3]\text{Cl}\cdot\text{PF}_6$ {R= (Me), ethyl (Et), *n*-propyl (*n*-Pr), *n*-butyl (*n*-Bu), and *n*-pentyl (*n*-Pen)} [21]. Once again N-H...Cl hydrogen bonds link the spin centres but this time the different alkyl groups result in a variety of supramolecular motifs giving both gradual and abrupt SCO accompanied by hysteresis. Interestingly, *fac*- $[\text{Fe}(2\text{-Me-4-ima-}n\text{Pr})_3]\text{Cl}\cdot\text{PF}_6$ shows scan rate dependence of the hysteresis but unlike $[\text{Fe}\{\text{N-}n\text{Bu-im}\}_3\text{-tren}]\text{(PF}_6)_2$ there are no phase changes [22]. Kruger and co-workers reported $[\text{Fe}(2\text{-ima-}p\text{-C}_6\text{H}_4\text{OMe})_3](\text{ClO}_4)_2$, a rare example of a *mer*-isomer [23]. In this case, π - π and C-H... π interactions and hydrogen bonds to the perchlorate anions link the Fe centres. However, the most interesting aspect of this complex is that it undergoes full switching under light irradiation [23]. Gu et al. have also investigated the impact of chirality on SCO in a series of complexes exemplified by *fac*- Λ - $[\text{Fe}(R\text{-N-Me-2-ima-CH}(\text{Me})\text{Ph})_3](\text{BF}_4)_2\cdot\text{MeCN}$ and *fac*- Δ - $[\text{Fe}(S\text{-N-Me-2-ima-CH}(\text{Me})\text{Ph})_3](\text{BF}_4)_2\cdot\text{MeCN}$ [24]. Racemisation of the stereogenic Fe(II) centre in the complexes is prevented by intramolecular π - π contacts between the imidazole and phenyl groups. In accordance with the identical packing arrangements both compounds exhibit moderately abrupt SCO. While the above shows there has been considerable research into imidazole based SCO systems aromatic groups remain poorly explored and in this work we report $[\text{Fe}(4\text{-ima-Bp})_3](\text{Y})_2\cdot\text{Sol}$ ($\text{Y} = \text{ClO}_4$; sol = EtOH 1, MeOH 2; $\text{Y} = \text{BF}_4$; sol = EtOH 3, MeOH 4 and MeCN 5) and investigate solvent and anion effects.

2. Materials and Methods

Perchlorate complexes are potentially explosive and should only be prepared in small quantities. 4-aminobiphenyl is a category 1 suspected carcinogen and facemasks and gloves must be used.

2.1. General Remarks

All manipulations were performed in air with reagent grade solvents. All chemicals were purchased from Aldrich Chemical Company (Singapore) or TCI Chemical Company (Tokyo, Japan) and used as received. Infrared spectra (as KBr discs) were recorded on a Perkin-Elmer Spectrum One infrared spectrophotometer in the range 400–4000 cm⁻¹. Electronic spectra were recorded in MeOH or MeCN at room temperature on a Shimadzu UV-1700 UV-VIS spectrophotometer (Kyoto, Japan). ¹H NMR spectra were recorded on a Bruker 300 MHz FT-NMR spectrometer (Karlsruhe, Germany) at

25 °C in CDCl₃ with SiMe₄ added as an internal standard. Elemental analyses were carried out on a Eurovector EA3000 analyser (Pavia, Italy). ESI-MS were carried out on a Bruker Daltonics 7.0T Apex 4 FTICR mass spectrometer (Karlsruhe, Germany).

2.1.1. Synthesis of 4-ima-Bp

4-ima-Bp was prepared by mixing 4-imidazolecarboxaldehyde (0.480 g, 5.0 mmol) and 4-aminobiphenyl (0.846 g, 5.0 mmol) in methanol (15 cm³). The mixture was warmed at ~50 °C under stirring for 1 h and then cooled to room temperature to give a pale yellow precipitate which was filtered. The pale yellow powder was dried in air, yield 1.194 g (97%). ν_{\max} (KBr)/cm⁻¹ 3123 w, 3054 w, 2948 w, 2787 m, 1621 s, 1585 s, 1485 m, 1456 m, 1329 m, 1119 s (Figure S1). λ_{\max} /nm (DMF, ϵ /M⁻¹cm⁻¹) 340 (970). ¹H NMR (CDCl₃, 295 K, 300 MHz) δ = 8.46 (s, 1H_f), 7.63 (s, 1H_h), 7.65-7.60 (m, 4H_{2d, 2e}), 7.48-7.31 (t, 2H_{2c}), 7.38-7.26 (m, 1H_{a, 2b, g}; Figure S2 Anal. Calc. for C₁₇H₁₄N₂O₂: C, 73.37; H, 5.07; N, 10.06. Found: C, 73.40; H, 5.12; N, 9.93%.

2.1.2. Synthesis of *fac*-[Fe(4-ima-Bp)₃](ClO₄)₂·3EtOH 1

The 4-ima-Bp ligand (0.148 g, 0.6 mmol) was dissolved in hot ethanol (3 cm³) and a EtOH solution (2 cm³) of Fe(ClO₄)₂·6H₂O (0.051 g, 0.2 mmol) was added dropwise with stirring to give a red solution. The mixture was stirred for 3 h and then cooled to room temperature to give dark red microcrystals of the product, which were dried in air, yield 0.106 g (53%). Red crystals suitable for single crystal X-ray diffraction were grown by slow evaporation of ethanol. *m/z* (ESI) 248.2 [4-ima-Bp]⁺, 795.9 [Fe(4-ima-Bp)₃]⁺, 895.5 [Fe(4-ima-Bp)₃][ClO₄]⁺, 99 [ClO₄]⁻. The microcrystals analyse for 2 equivalents of EtOH and 1 equivalent of water. Anal. Calc. for C₅₂H₅₃N₉O₁₁Cl₂Fe: C, 56.41; H, 4.83; N, 11.39. Found: C, 56.06; H, 4.54; N, 11.60%.

2.1.3. Synthesis of *fac*-[Fe(4-ima-Bp)₃](ClO₄)₂·3MeOH 2

The compound was made in a similar way to **1** using MeOH instead of EtOH giving dark red microcrystals, yield 0.217 g (67%). *m/z* (ESI) 248.2 [4-ima-Bp]⁺, 557.2 [Fe(4-ima-Bp)₂]⁺, 795.9 [Fe(4-ima-Bp)₃]⁺, 99 [ClO₄]⁻. Anal. Calc. for C₅₁H₅₁N₉O₁₁Cl₂Fe: C, 56.04; H, 4.71; N, 11.54. Found: C, 56.55; H, 4.65; N, 11.71%.

2.1.4. Synthesis of *fac*-[Fe(4-ima-Bp)₃](BF₄)₂·EtOH·4H₂O 3

The compound was made in a similar way to **1** using Fe(BF₄)₂·6H₂O instead of Fe(ClO₄)₂·6H₂O giving dark red microcrystals, yield 0.150 g (77%). *m/z* (ESI) 248.2 [4-ima-Bp]⁺, 557.2 [Fe(4-ima-Bp)₂]⁺, 795.9 [Fe(4-ima-Bp)₃]⁺, 87 [BF₄]⁻. Anal. Calc. for C₅₂H₄₇N₉B₂F₈O₅Fe: C, 56.36; H, 4.28; N, 11.38. Found: C, 56.11; H, 4.60; N, 11.56%.

2.1.5. Synthesis of *fac*-[Fe(4-ima-Bip)₃](BF₄)₂·4H₂O 4

The compound was made in a similar way to **3** using MeOH instead of EtOH giving red microcrystals yield 0.113 g (57%). *m/z* (ESI) 248.2 [4-ima-Bp]⁺, 557.2 [Fe(4-ima-Bp)₂]⁺, 795.9 [Fe(4-ima-Bp)₃]⁺, 87 [BF₄]⁻. Anal. Calc. for C₄₈H₄₇N₉F₈B₂O₄Fe: C, 55.21; H, 4.54; N, 12.08. Found: C, 54.93; H, 4.45; N, 11.90%.

2.1.6. Synthesis of *fac*-[Fe(4-ima-Bip)₃](BF₄)₂·3.5MeCN 5

Red crystals of the compound were made by dissolving 0.05 mmol of **3** in acetonitrile (5 cm³) and allowing slow diffusion of Et₂O into the solution yielding red single crystals, 0.043 g (83%). *m/z* (ESI) 248.2 [4-ima-Bp]⁺, 557.2 [Fe(4-ima-Bp)₂]⁺, 87 [BF₄]⁻. The compound analyses for 3 equivalents of MeCN. Anal. Calc. for C₅₄H₄₈N₁₂B₂F₈Fe: C, 59.22; H, 4.42; N, 15.56. Found: C, 59.11; H, 4.37; N, 15.40%.

2.2. VSM and SQUID Magnetometry Studies

Magnetic susceptibility data on **1-4** were collected on a Quantum Design Versalab Measurement System with a vibrating sample magnetometer (VSM) attachment within a small-bore hole cavity. Samples were contained within a polypropylene holder and held within a brass half-tube designed for VSM measurements. Measurements were taken continuously under an applied field of 0.3 T over the temperature range 300–50–300 K, at a ramp rate of 1 K min^{−1} with no overshoot. Magnetic susceptibility data on **5** was collected on either a Quantum Design MPMS 5 or a MPMS XL-7 SQUID magnetometer (San Diego, USA) at a scan rate of 10 K·min^{−1} being careful to allow long equilibrium times at each data point. All samples were taken freshly from the mother liquor in which the crystals were grown to limit any potential solvent loss. The raw data was corrected for the sample holder and diamagnetic contributions.

2.3. X-ray Crystallography

Crystal data and data processing parameters for the structures of **1**, **2** and **5** are given in Table 1. X-ray quality crystals of **1** and **2** were grown by slow evaporation of the solvent. Crystals were mounted on a glass fibre using perfluoropolyether oil and cooled rapidly to 100 K in a stream of cold nitrogen. The diffraction data of **1** and **2** were collected at 143 and 153 K on a Rigaku Spider diffractometer equipped with a MicroMax MM007 rotating anode generator, Cu_α radiation ($\lambda = 1.54178 \text{ \AA}$), high-flux Osmic multilayer mirror optics, and a curved image-plate detector. The data were integrated, scaled and averaged with FS Process [25]. Diffraction data for **5** were collected at 123 K on a Bruker APEXII area detector with graphite monochromated MoK α ($\lambda = 0.71073 \text{ \AA}$) [26]. After data collection, in each case an empirical absorption correction was applied [27]. The structures were then solved by direct methods and refined on all F^2 data using the SHELX suite of programs [28,29]. In all cases non-hydrogen atoms were refined with anisotropic thermal parameters; hydrogen atoms were included in calculated positions and refined with isotropic thermal parameters which were *ca.* 1.2 × (aromatic CH) or 1.5 × (CH₂, Me) the equivalent isotropic thermal parameters of their parent carbon atoms. All pictures were generated using Olex2 [30]. The CCDC numbers for the X-ray crystallographic data presented in this paper are 18925687-1892569 and can be obtained free of charge from the Cambridge Crystallographic Data Centre via www.ccdc.cam.ac.uk/data_request/cif.

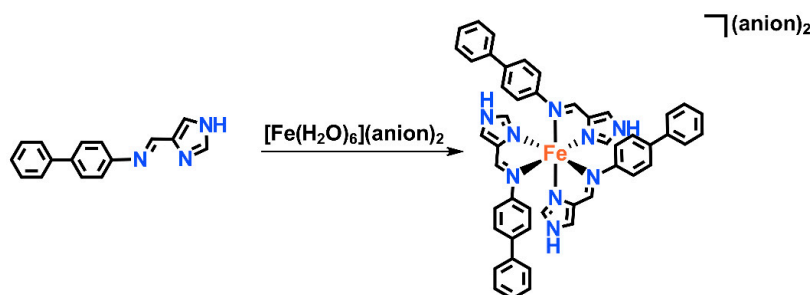
Table 1. Crystallographic data and structure refinement for **1**, **2** and **5**.

Compound	1	2	5
Formula	C ₅₄ H ₅₇ Cl ₂ FeN ₉ O ₁₁	C ₅₁ H ₅₁ Cl ₂ FeN ₉ O ₁₁	C _{55.5} H _{49.5} B ₂ FeN _{12.5} F ₈
Molecular weight/gmol ^{−1}	1134.83	1092.76	1080.04
Crystal system	Trigonal	Trigonal	Triclinic
Space group	R $\bar{3}$	R $\bar{3}$	P $\bar{1}$
<i>a</i> /Å	13.1242(9)	12.9080(15)	13.0204(7)
<i>b</i> /Å	13.1242(9)	12.9080(15)	13.1932(8)
<i>c</i> /Å	53.258(4)	52.5240(4)	18.4021(11)
α /°	90	90	73.540(4)
β /°	90	90	86.375(4)
γ /°	120	120	61.569(3)
T/K	143(2)	153(2)	123(2)
Cell volume/Å ³	7944.4(12)	7578.9(18)	2656.3(3)
Z	6	6	4
Absorption coefficient/mm ^{−1}	3.797	3.958	0.363
Reflections collected	23981	19730	39419
Independent reflections, R_{int}	3413, 0.094	2875, 0.092	9354, 0.0825
Max. and min. transmission	0.561, 1.000	1.000 and 0.772	-
Restraints/parameters	2/206	0/224	0/878
Final R indices [$I > 2\sigma(I)$]: R_1 , wR_2	0.1383, 0.3738	0.122, 0.392	0.1142, 0.2301
CCDC no.	1892568	1892567	1892569

3. Results

3.1. Synthesis and Characterization of *fac*-[Fe(4-*ima*-Bp)₃](Y)₂·sol Complexes

The synthesis of a family of *fac*-[Fe(4-*ima*-Bp)₃](Y)₂·sol complexes was achieved by a reaction between the 4-*ima*-Bp ligand in MeOH or EtOH and Fe(ClO₄)₂·XH₂O or Fe(BF₄)₂·6H₂O which affords dark red powders of the octahedral complexes *fac*-[Fe(4-*ima*-Bp)₃](Y)₂·sol (Y = ClO₄; sol = 3EtOH **1**, 3MeOH **2**; Y = BF₄; sol = EtOH·4H₂O **3**, 4H₂O **4** and 3.5MeCN **5**), Scheme 1. The acetonitrile solvate, **5** was prepared by recrystallization of **3** from MeCN/Et₂O.



Scheme 1. Synthesis of *fac*-[Fe(4-*ima*-Bp)₃](Y)₂·sol.

3.2. IR and UV–VIS Spectroscopy

IR spectroscopy of **1–5** shows an imine stretch at 1620 cm⁻¹ and at lower wavenumbers than the free ligand consistent with coordination to the metal (Table 2) [16,24,31]. Bands for the anions are also clearly visible in their expected positions (1083 and 1087 cm⁻¹). The presence of a further set of bands between 3362–3377 cm⁻¹ are consistent with O–H stretches suggesting that EtOH, MeOH or H₂O is present in the structures of these compounds.

Table 2. Physical and IR spectroscopic data for *fac*-[Fe(4-*ima*-Bp)₃](Y)₂·sol.

Compound	%yield	Colour	IR (cm ⁻¹)				
			$\nu_{C=N}$	$\nu_{C=C}$	ν_{OH}	ν_{ArH}	ν_{anion}
1 (ClO ₄ ·3EtOH)	53	Dark red	1620	1484	3362	3128	1087
2 (ClO ₄ ·3EtOH)	67	Dark red	1621	1484	3380	3135	1089
3 (BF ₄ ·EtOH·4H ₂ O)	77	Dark red	1620	1484	3377	3137	1083
4 (BF ₄ ·4H ₂ O)	57	Dark red	1620	1484	3377	3137	1083
5 (BF ₄ ·3.5MeCN)	63	Red Orange	1620	1484	-	3144	1051

In the visible region a DMF solution of 4-*ima*-Bp reveals an absorbance maximum at 340 nm ($\epsilon = 24000 \text{ M}^{-1}\text{cm}^{-1}$) which arises from an intraligand $\pi \rightarrow \pi^*$ transition (Table 3) [32]. At room temperature, methanol solutions of **1–4** are orange and exhibit $\pi \rightarrow \pi^*$ transitions at approximately 330 and 280 nm (Figure 1). UV–VIS spectra of **1** and **3** in MeCN (in which **1–4** are more soluble), as representative examples of the compounds, reveal a possible band at *ca.* 840 nm consistent with the compounds being HS in solution (Figure S3).

Table 3. Wavelength maxima and extinction coefficients of *fac*-[Fe(4-*ima*-Bp)₃](Y)₂ in MeOH.

Compound	λ_{max}/nm ($\epsilon_{max}/\text{M}^{-1}\text{cm}^{-1}$)
1	328 (65,000), 283 (72,000)
2	326 (57,000), 283 (50,000)
3	327 (66,200), 283 (61,000)
4	328 (56,000), 283 (51,000)

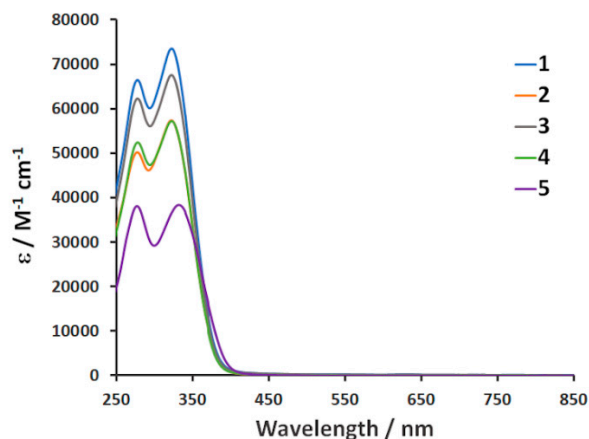


Figure 1. UV-VIS spectra of *fac*-[Fe(4-ima-Bp)₂](Y)₂·sol **1–5** in MeOH.

3.3. Structural Studies of *fac*-[Fe(4-ima-Bp)₃](Y)₂·sol Complexes

The structure of *fac*-[Fe(4-ima-Bp)₃](ClO₄)₂·3EtOH **1** determined by single-crystal X-ray diffraction at 143 K shows the compound reveals a trigonal symmetry (space group $R\bar{3}$, Figure 2). The methanol solvate **2**, is isostructural to **1** (collected at 153 K). The asymmetric units contain the Fe centre, a single 4-ima-Bp ligand, parts of two perchlorate anions and an EtOH (partially disordered in **1**) or MeOH molecule. The ligands coordinate with a facial (*fac*) disposition around the metal centre. In contrast, *fac*-[Fe(4-ima-Bp)₃](BF₄)₂·3.5MeCN **5** crystallizes in the triclinic $P\bar{1}$ space group. Despite the change in symmetry and the different anion the general features of **5** are remarkably similar to those of **1** and **2**. The Fe-ligand bond lengths and octahedral distortion parameters for **1**, **2** and **5** are given in Table 4. Comparison with [Fe(2-Me-4-ima-*n*Pr)₃](Cl·Y) [22,31] and [Fe(*N*-Me-2-ima-CH(Me)Ph)₃](BF₄)₂·MeCN [24] indicates that the Fe(II) centres are LS at the low temperature used for X-ray data collection. Interestingly, in **1** and **2** the bond lengths are shorter by ca. 0.03 Å than the LS centre in [Fe(2-ima-*p*-C₆H₄OMe)₃](ClO₄)₂—the only other previously reported mononuclear system where the aromatic group is directly connected to the imine nitrogen [23]. The octahedral distortion parameters are also consistent with LS centres.

Table 4. Selected bond lengths, octahedral distortion parameters and hydrogen bonding distances (Å, °) for **1**, **2** and **5**.

Bond lengths	1-143 K	2-153 K		5-123 K
Fe1–N1	1.962(6)	1.964(8)	Fe1–N1	1.971(4)
	-	-	Fe1–N3	1.995(4)
	-	-	Fe1–N4	1.962(4)
Fe1–N3	2.005(5)	1.983(8)	Fe1–N6	1.992(4)
	-	-	Fe1–N7	1.963(4)
	-	-	Fe1–N9	2.001(4)
Σ [33]	68.7	55.7		57.9
Θ [34]	196.4	127.3		125.0
N2-H2...O5	1.829(9)	1.832(11)	N8-H8...F3	2.109(4)
O5-H5...O4	-	2.09(2)	N8-H8...F2	2.426(4)
			N5-H5...F1	1.939(4)
			N2-H2...N10	2.041(5)

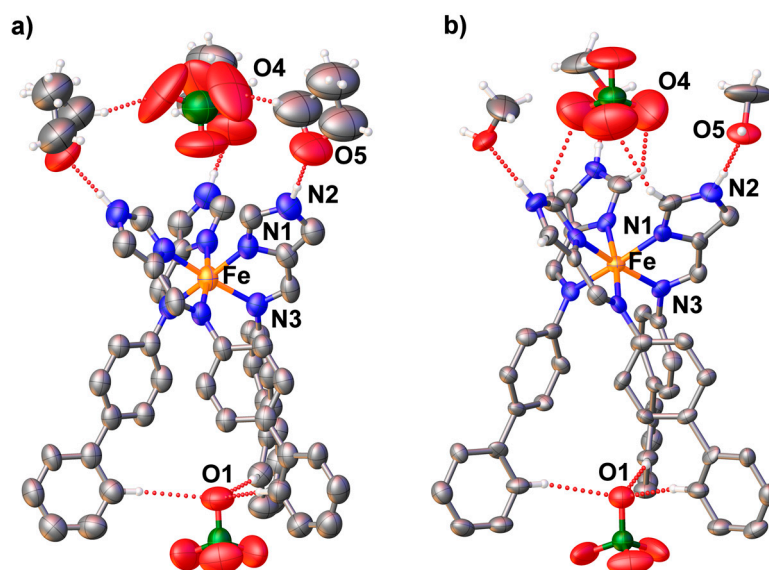


Figure 2. View of the molecular unit of (a) **1** and (b) **2**. Only selected hydrogen atoms and labels are shown in the interests of clarity. Ellipsoids are drawn at 50% probability.

A particular feature of the structures is that one of the anions sits in a pocket of biphenyl groups and is held in place by three C–H···O interactions (see Figure 2). The pocket is reinforced by three *intramolecular* C–H··· π contacts, Figure 3. The imidazole hydrogens are involved in H-bonding to the solvent and not the anion as is seen in systems like [Fe(2-Me-4-ima-*n*Pr)₃]Cl·Y. The second perchlorate anion instead forms H-bonds to the solvent molecules and weaker C–H···O interactions involving either ethanol or imidazole C–H groups. This change in packing at the second anion results in an inversion of the perchlorate in **1** compared with **2** (Figure 2).

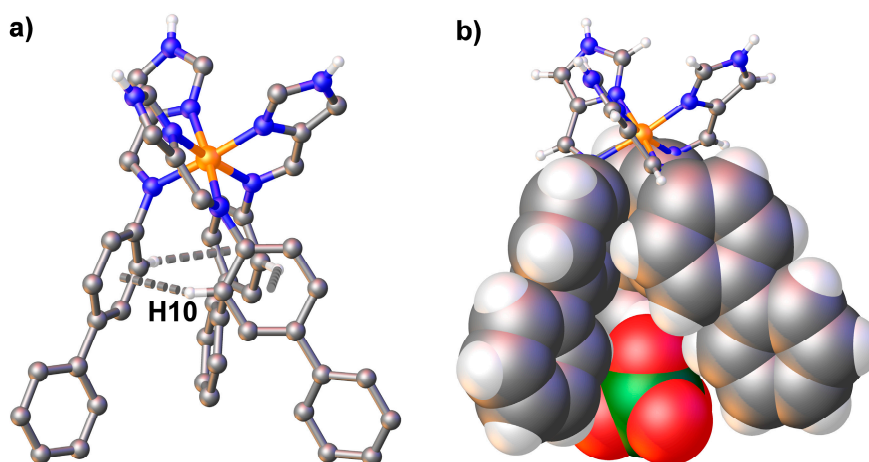


Figure 3. View of (a) the *intramolecular* C–H··· π contacts in **1** and (b) spacefill diagram showing the perchlorate anion in the biphenyl pocket.

The overall packing for both compounds involves multiple C–H··· π interactions of the propeller like biphenyl arms forming a triangular motif (Figure 4; Table S1). Within each ‘triangle’ of *fac*-[Fe(4-ima-Bp)₃]²⁺ cations the Fe centres are chiral but as the intercalated triangle is of the opposite hand the overall structure is achiral, as expected. There are also C–H··· π interactions between the Λ and Δ *fac*-[Fe(4-ima-Bp)₃]²⁺ cations giving rise to a hexagonal motif (Figure 4b). As this is present in all the compounds in this series it is clearly very robust.

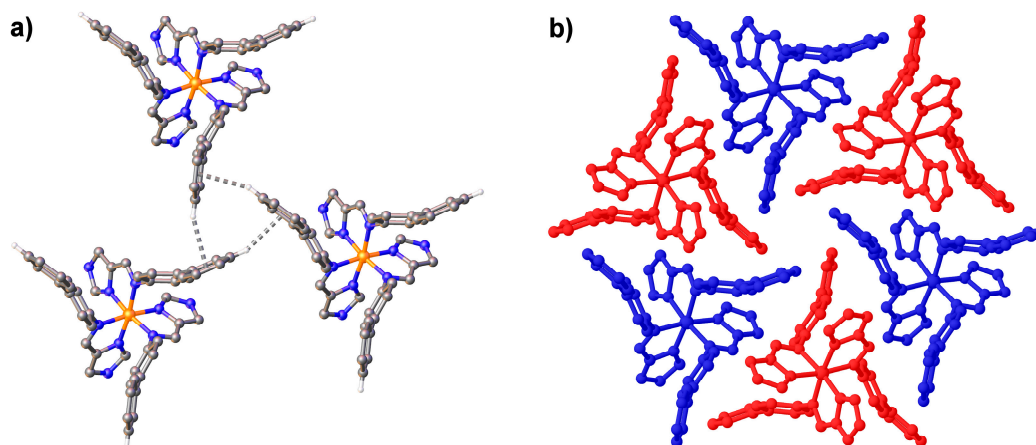


Figure 4. View of the (a) intermolecular C–H... π interactions that link the (b) Λ (blue) and Δ (red) fac -[Fe(4-ima-Bp)₃]²⁺ cations that form the hexagonal motif in **1**.

The hexagonal planes are approximately 12.5 Å thick and are separated from each other by an extensive network of perchlorate anions and the MeOH or EtOH solvent molecules held together by N–H...O and O–H...O hydrogen bonds (Figure 5; Figure S4). Similar 2D layers are present in the imidazolyl-imine dimers, [Fe(2-Me-ima-N-N-ima-2-Me)₃](ClO₄)₄ [32].

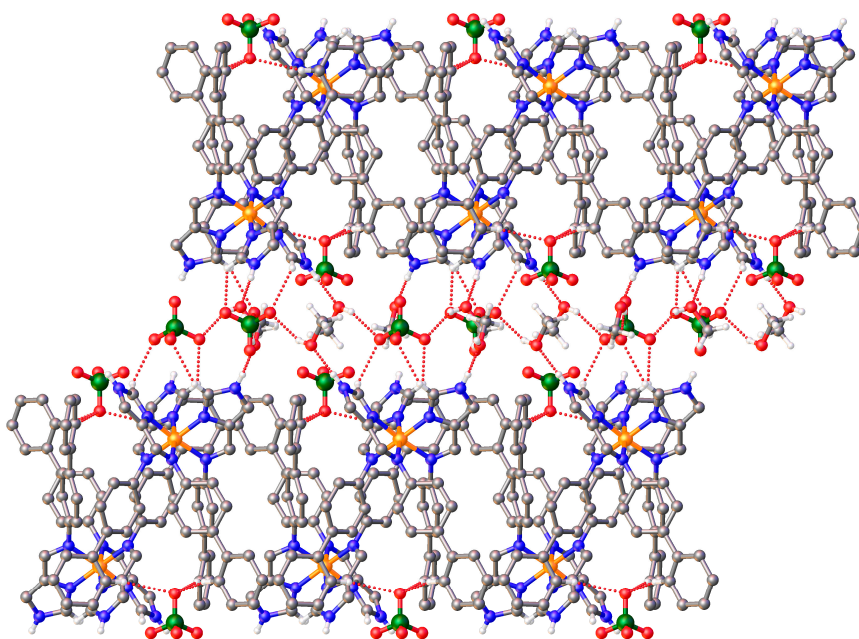


Figure 5. Side-on view of the 2D hexagonal planes and the ClO₄-MeOH layer in **2** that links the planes.

As noted above, the structure of the MeCN solvate **5** is very similar to **1** and **2**. A particular difference is that the BF₄[−] anion directly links the 2D layers of the fac -[Fe(4-ima-Bp)₃]²⁺ cations through N–H...F hydrogen bonds. The remaining imidazole N–H group is hydrogen bonded to one of the acetonitrile molecules. A combination of C–H...N/F interactions hold the remaining MeCN molecules in the anion-solvent layer. The other subtle difference is that the 2D layers are no longer hexagonal, but are instead slightly distorted (Figures S5 and S6). This has a number of consequences including the loss of some C–H... π interactions and the concomitant formation of slightly angular π - π interactions (Figure 6). We also observe a reduction in the gap between the layers from ca. 13 Å in **1** and **2** to 10.8 Å in **5**.

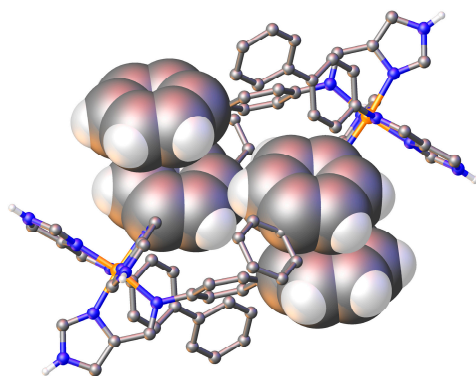


Figure 6. View of the π - π interactions in *fac*-[Fe(4-ima-Bp)₃](BF₄)₂·3.5MeCN **5**.

3.4. Magnetic studies of [Fe(4-ima-Bp)₃](Y)₂·sol Complexes

The magnetic properties of **1–5** have been studied by magnetic susceptibility (see $\chi_M T$ versus T plots, Figures 7 and 8). All the compounds except **1** show a complete HS to LS transition around room temperature. The exception is **1** which shows a SCO profile that is more abrupt than **2** in the first warming (Figure S7) but thereafter exhibits a more gradual crossover with $\chi_M T$ going from 1.7 cm³·mol⁻¹·K to 3.3 cm³·mol⁻¹·K between 150 K and 350 K; indicating a 50% transition from the HS to LS state. Notably, the first measurement in **1** shows hysteresis, but this is only apparent, with the SCO profile changing upon subsequent cycles to finally give the profile shown in Figure 7. The change in SCO behaviour in **1** has been shown by TGA studies to be due to loss of one equivalent of EtOH (Figure S8). Similar solvent loss has been observed in *fac*-[Fe(N-Me-2-ima-CH(Me)Ph)₃](BF₄)₂·MeCN and also lowers the transition temperature [24]. Interestingly, despite the different solvents and anions **2–4** show very similar SCO profiles with $T_{1/2}$ varying slightly between 305 and 320 K. It is important to state that we cannot absolutely rule out solvent loss in the case of **2–5**, but the fact that we measured several thermal cycles with no change in the SCO profile seems to suggest that this is unlikely. We also note that the initial SCO profile in **5** is more gradual in the first 200 K, the exact reason for this behaviour is unclear but it is repeatable. Although we have been unable to obtain the structures of **3** and **4**, these results suggest that the hexagonal motif noted in Figure 4 is also present in **3** and **4** hence the almost identical SCO profiles observed. This is supported by the fact that in **5** the packing becomes *pseudo*-hexagonal and the SCO is now less abrupt and occurs at a slightly lower temperature. A comparison with [Fe(2-ima-*p*-C₆H₄OMe)₃](ClO₄)₂ which exhibits a complete spin crossover at 158 K [23] suggests that the biphenyl group, despite its size, stabilizes the LS state more than in [Fe(2-ima-*p*-C₆H₄OMe)₃](ClO₄)₂.

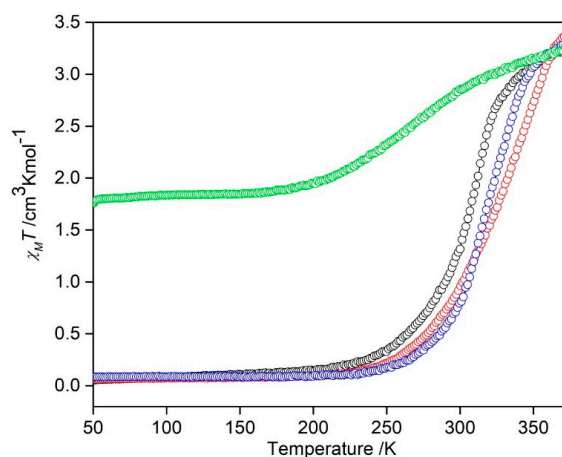


Figure 7. VSM profiles of *fac*-[Fe(4-ima-Bp)₃](Y)₂·sol as $\chi_M T$ vs. T plots of a) **1** (green), b) **2** (red), c) **3** (blue) and d) **4** (black).

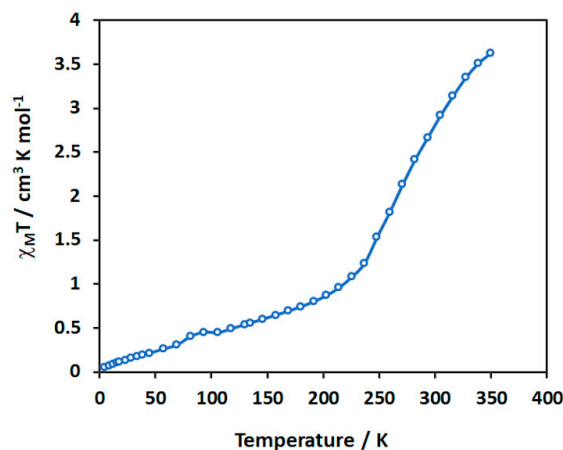


Figure 8. SQUID profile of *fac*-[Fe(4-ima-Bp)₃](BF₄)₂·3.5MeCN 5.

3.5. Thermochromism

The complexes 1–4 all undergo a clear and reversible colour change from dark red to orange in the solid state with heating (Figure 9) associated with a LS to HS transition. Reports on thermochromism in Fe(II) imidazolyl complexes are rare and this colour change is different from the *fac*-[Fe(2-Me-4-ima-R)₃]Cl·PF₆ series where a change from yellow to orange/red is observed [35]. It follows that the R group on the imine nitrogen can be used to tune the thermochromic behaviour of such SCO systems. In addition, we have soaked filter paper in a solution of 2 and find that it reversibly changes colour from red to yellow between 30 and 60 °C (see supplementary video).

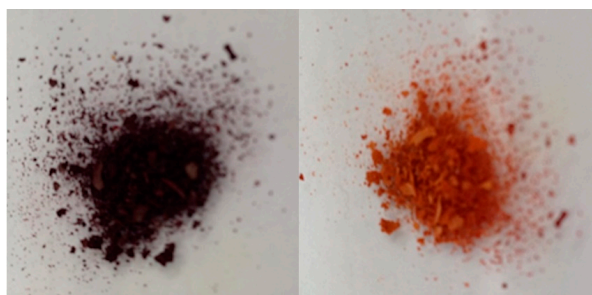


Figure 9. Colour change of *fac*-[Fe(4-ima-Bp)₃](ClO₄)₂·3MeOH 1 heating from 298 K (left) to 423 K (right).

4. Conclusions

In conclusion, we have prepared five Fe(II) complexes of the new 4-ima-Bp ligand and a variety of anions and solvent molecules. Structural studies show that all compounds crystallize as the *fac* isomer probably due to *intramolecular* C–H···π contacts involving the biphenyl groups and trapping of one of the anions. 2D hexagonal or *pseudo*-hexagonal layers of the *fac*-[Fe(4-ima-Bp)₃]²⁺ cations form principally through C–H···π interactions. Strong hydrogen bonding between the layers is facilitated by the anions and solvent molecules giving rise to a high transition temperature, but moderately gradual SCO transitions. Notably, the solvent is found to influence SCO behaviour more than the anion. Moreover, the biphenyl group allows tuning of the spin transition temperature and represents a promising strategy in the design of more abrupt SCO systems that will operate at room temperature.

Supplementary Materials: The following are available online at <http://www.mdpi.com/2073-4352/9/2/116/s1>, Figure S1. IR spectra of 1–4. Figure S2. ¹H-NMR spectrum of 4-ima-Bp. Figure S3. UV–VIS of [Fe(4-ima-Bp)₃](ClO₄)₂ 1 and [Fe(4-ima-Bp)₃](BF₄)₂ 3 in MeCN in a 0.1 M solution. Figure S4. Side-on view of the packing in *fac*-[Fe(4-ima-Bp)₃](ClO₄)₂·3MeOH 2. Figure S5. View of the *pseudo*-hexagonal packing motif in *fac*-[Fe(4-ima-Bp)₃](BF₄)₂·3.5MeCN 5. Figure S6. Comparative view of the hexagonal and *pseudo*-hexagonal packing motifs found in 2 and 5. Figure S7. SQUID profile of *fac*-[Fe(4-ima-Bp)₃](ClO₄)₂·3EtOH 1. Figure S8.

TGA of *fac*-[Fe(4-*ima*-Bp)₃](ClO₄)₂·3EtOH **1**. Table S1. Geometric parameters of C–H···π and π–π interactions in **1–2** and **5**. A supplementary video showing the thermochromism in **2**.

Author Contributions: P.H. and D.J.H. designed, administered and supervised the project. P.H. and D.J.H. wrote the manuscript with input from all other authors. D.S. synthesized all compounds, and collected and analysed spectroscopic and crystallographic data; the latter for **5**. K.S.M. and B.M. conducted all SQUID magnetometry measurements. S.M.N. collected and analysed all VSM data. L.L. and S.G.T. collected and solved the structures for **1** and **2**.

Funding: We thank the Thailand Research Fund (grant nos. RSA5580028, BRG6180008) for funding this research and financial support from the Thailand Research Fund in the form of a Royal Golden Jubilee scholarship to DS (PHD/0135/2554).

Conflicts of Interest: The authors declare no conflict of interest.

References

1. *Spin-Crossover Materials: Properties and Applications*; Halcrow, M.A. (Ed.) John Wiley & Sons Ltd.: Chichester, UK, 2013.
2. Gütlich, P.; Goodwin, H.A. Spin Crossover—An Overall Perspective. *Top. Curr. Chem.* **2004**, *233*, 1–47.
3. Boillot, M.L.; Weber, B. Mononuclear ferrous and ferric complexes. *Comptes Rendus Chim.* **2018**, *21*, 1196–1208. [[CrossRef](#)]
4. Collet, E.; Guionneau, P. Structural analysis of spin-crossover materials: From molecules to materials. *Comptes Rendus Chim.* **2018**, *21*, 1133–1151. [[CrossRef](#)]
5. Craig, G.A.; Roubeau, O.; Aromí, G. Spin state switching in 2,6-bis(pyrazol-3-yl)pyridine (3-bpp) based Fe(II) complexes. *Coord. Chem. Rev.* **2014**, *269*, 13–31. [[CrossRef](#)]
6. Brooker, S. Spin crossover with thermal hysteresis: practicalities and lessons learnt. *Chem. Soc. Rev.* **2015**, *44*, 2880–2892. [[CrossRef](#)] [[PubMed](#)]
7. Halcrow, M.A. Structure: function relationships in molecular spin-crossover complexes. *Chem. Soc. Rev.* **2011**, *40*, 4119–4142. [[CrossRef](#)] [[PubMed](#)]
8. Létard, J.-F.; Guionneau, P.; Goux-Capes, L. Towards Spin Crossover Applications. *Top. Curr. Chem.* **2004**, *235*, 221–249.
9. Senthil, K.; Ruben, M. Emerging trends in spin crossover (SCO) based functional materials and devices. *Coord. Chem. Rev.* **2017**, *346*, 176–205. [[CrossRef](#)]
10. Miller, R.G.; Brooker, S. Reversible quantitative guest sensing via spin crossover of an iron(ii) triazole. *Chem. Sci.* **2016**, *7*, 2501–2505. [[CrossRef](#)]
11. Létard, J.-F. Photomagnetism of iron(II) spin crossover complexes the T(LIESST) approach. *J. Mater. Chem.* **2006**, *16*, 2550–2559. [[CrossRef](#)]
12. Chastanet, G.; Desplanches, C.; Baldé, C.; Rosa, P.; Marchivie, M.; Guionneau, P. A critical review of the T(LIESST) temperature in spin crossover materials—What it is and what it is not. *Chem. Sq.* **2018**, *2*, 2. [[CrossRef](#)]
13. Scott, H.S.; Staniland, R.W.; Kruger, P.E. Spin crossover in homoleptic Fe(II) imidazolylimine complexes. *Coord. Chem. Rev.* **2018**, *362*, 24–43. [[CrossRef](#)]
14. Sunatsuki, Y.; Kawamoto, R.; Fujita, K.; Maruyama, H.; Suzuki, T.; Ishida, H.; Kojima, M.; Iijima, S.; Matsumoto, N. Structures and spin states of mono- and dinuclear iron(II) complexes of imidazole-4-carbaldehyde azine and its derivatives. *Coord. Chem. Rev.* **2010**, *254*, 1871–1881. [[CrossRef](#)]
15. Yamada, M.; Ooidemizu, M.; Ikuta, Y.; Osa, S.; Matsumoto, N.; Iijima, S.; Kojima, M.; Dahan, F.; Tuchagues, J.P. Interlayer Interaction of Two-Dimensional Layered Spin Crossover Complexes [Fe^{II}H₃LMe][Fe^{II}LMe]X (X = ClO₄[−], BF₄[−]). *Inorg. Chem.* **2003**, *42*, 8406–8416. [[CrossRef](#)] [[PubMed](#)]
16. Bréfuel, N.; Watanabe, H.; Toupet, L.; Come, J.; Matsumoto, N.; Collet, E.; Tanaka, K.; Tuchagues, J.-P. Concerted spin crossover and symmetry breaking yield three thermally and one light-induced crystallographic phases of a molecular material. *Angew. Chem. Int. Ed.* **2009**, *48*, 9304–9307. [[CrossRef](#)] [[PubMed](#)]
17. Yamada, M.; Hagiwara, H.; Torigoe, H.; Matsumoto, N.; Kojima, M.; Dahan, F.; Tuchagues, J.P.; Re, N.; Iijima, S. A variety of spin-crossover behaviors depending on the counter anion: Two-dimensional complexes constructed by NH···Cl-hydrogen bonds, [Fe^{II}H₃LMe]Cl·X (X = PF₆[−], AsF₆[−], SbF₆[−], CF₃SO₃[−]; H₃LMe = tris[2-((2-methylimidazol-4-yl)methylidene)amino]ethylamine). *Chem. Eur. J.* **2006**, *12*, 4536–4549. [[CrossRef](#)] [[PubMed](#)]

18. Seredyuk, M.; Muñoz, M.C.; Castro, M.; Romero-Morcillo, T.; Gaspar, A.B.; Real, J.A. Unprecedented multi-stable spin crossover molecular material with two thermal memory channels. *Chem. Eur. J.* **2013**, *19*, 6591–6596. [[CrossRef](#)] [[PubMed](#)]
19. Delgado, T.; Tissot, A.; Guénée, L.; Hauser, A.; Valverde-Muñoz, F.J.; Seredyuk, M.; Real, J.A.; Pillet, S.; Bendeif, E.-E.; Besnard, C. Very Long-Lived Photogenerated High-Spin Phase of a Multistable Spin-Crossover Molecular Material. *J. Am. Chem. Soc.* **2018**, *140*, 12870–12876. [[CrossRef](#)] [[PubMed](#)]
20. Nishi, K.; Arata, S.; Matsumoto, N.; Iijima, S.; Sunatsuki, Y.; Ishida, H.; Kojima, M. One-dimensional Spin-crossover iron(II) complexes bridged by intermolecular imidazole-pyridine NH \cdots N hydrogen bonds, [Fe(HLMe) $_3$] X_2 (HLMe = (2-Methylimidazol-4-yl-methylideneamino-2-ethylpyridine; X = PF $_6^-$, ClO $_4^-$, BF $_4^-$). *Inorg. Chem.* **2010**, *49*, 1517–1523. [[CrossRef](#)]
21. Nishi, K.; Matsumoto, N.; Iijima, S.; Halcrow, M.A.; Sunatsuki, Y.; Kojima, M. A hydrogen bond motif giving a variety of supramolecular assembly structures and spin-crossover behaviors. *Inorg. Chem.* **2011**, *50*, 11303–11305. [[CrossRef](#)]
22. Fujinami, T.; Nishi, K.; Hamada, D.; Murakami, K.; Matsumoto, N.; Iijima, S.; Kojima, M.; Sunatsuki, Y. Scan Rate Dependent Spin Crossover Iron(II) Complex with Two Different Relaxations and Thermal Hysteresis fac-[FeII(HLn-Pr) $_3$]Cl·PF $_6$ (HLn-Pr = 2-Methylimidazol-4-yl-methylideneamino-n-propyl). *Inorg. Chem.* **2015**, *54*, 7291–7300. [[CrossRef](#)] [[PubMed](#)]
23. Thompson, J.R.; Archer, R.J.; Hawes, C.S.; Ferguson, A.; Wattiaux, A.; Mathonière, C.; Clérac, R.; Kruger, P.E. Thermally and photo-induced spin crossover behaviour in an Fe(II) imidazolylimine complex: [FeL $_3$](ClO $_4$) $_2$. *Dalton Trans.* **2012**, *41*, 12720–12725. [[CrossRef](#)] [[PubMed](#)]
24. Gu, Z.-G.; Pang, C.-Y.; Qiu, D.; Zhang, J.; Huang, J.-L.; Qin, L.-F.; Sun, A.-Q.; Li, Z. Homochiral iron(II) complexes based on imidazole Schiff-base ligands: Syntheses, structures, and spin-crossover properties. *Inorg. Chem. Commun.* **2013**, *35*, 164–168. [[CrossRef](#)]
25. Rigaku. *Rigaku XRD*; Rigaku Corporation: Tokyo, Japan, 1996.
26. Bruker APEXII; Bruker AXS Inc.: Madison, WI, USA, 2005.
27. SAINT and SADABS; Bruker AXS Inc.: Madison, WI, USA, 2003.
28. Sheldrick, G.M. Crystal structure refinement with SHELXL. *Acta Crystallogr. Sect. C Struct. Chem.* **2015**, *71*, 3–8. [[CrossRef](#)] [[PubMed](#)]
29. Sheldrick, G.M. SHELXT-Integrated space-group and crystal-structure determination. *Acta Crystallogr. Sect. A Found. Crystallogr.* **2015**, *71*, 3–8. [[CrossRef](#)] [[PubMed](#)]
30. Dolomanov, O.V.; Bourhis, L.J.; Gildea, R.J.; Howard, J.A.K.; Puschmann, H. OLEX2: a complete structure solution, refinement and analysis program. *J. Appl. Cryst.* **2009**, *42*, 339–342. [[CrossRef](#)]
31. Fujinami, T.; Nishi, K.; Matsumoto, N.; Iijima, S.; Halcrow, M.A.; Sunatsuki, Y.; Kojima, M. 1D and 2D assembly structures by imidazole \cdots chloride hydrogen bonds of iron(II) complexes [Fe^{II}(HLn-Pr) $_3$]Cl·Y (HLn-Pr = 2-methylimidazol-4-yl-methylideneamino-n-propyl; Y = AsF $_6^-$, BF $_4^-$) and their spin states. *Dalton Trans.* **2011**, *40*, 12301–12309. [[CrossRef](#)]
32. Sunatsuki, Y.; Kawamoto, R.; Fujita, K.; Maruyama, H.; Suzuki, T.; Ishida, H.; Kojima, M.; Iijima, S.; Matsumoto, N. Structures and spin states of bis(tridentate)-type mononuclear and triple helicate dinuclear iron(II) complexes of imidazole-4-carbaldehyde azine. *Inorg. Chem.* **2009**, *48*, 8784–8795. [[CrossRef](#)]
33. McCusker, J.K.; Rheingold, A.L.; Hendrickson, D.N. Variable-Temperature Studies of Laser-Initiated 5T_2 to 1A_1 Intersystem Crossing in Spin-Crossover Complexes: Empirical Correlations between Activation Parameters and Ligand Structure in a Series of Polypyridyl Ferrous Complexes. *Inorg. Chem.* **1996**, *35*, 2100–2112. [[CrossRef](#)]
34. Marchivie, M.; Guionneau, P.; Létard, J.F.; Chasseau, D. Photo-induced spin-transition: the role of the iron(II) environment distortion. *Acta Crystallogr. Sect. B Struct. Sci.* **2005**, *61*, 25–28. [[CrossRef](#)]
35. Furushou, D.; Hashibe, T.; Fujinami, T.; Nishi, K.; Hagiwara, H.; Matsumoto, N.; Sunatsuki, Y.; Kojima, M.; Iijima, S. Reprint of "facial and meridional geometrical isomers of tris(2-methylimidazol-4-yl-methylideneaminobenzyl)iron(II) with delta- and lambda-configurations and their enantio-discriminative assembly via imidazole \cdots chloride hydrogen bonding and spin crossover. *Polyhedron* **2012**, *44*, 194–203. [[CrossRef](#)]

